U. S. AIR FORCE

PROJECT RAND

RESEARCH MEMORANDUM

BOUNDARY LAYER DRAG FOR NON-SMOOTH SURFACES

W. W. Gollos

RM-1129

24 June 1953

Assigned to _____

This is a working paper. It may be expanded, modified, or withdrawn at any time. The views, conclusions, and recommendations expressed herein do not necessarily reflect the official views or policies of the United States Air Force.

The RAND Corporation
1700 MAIN ST. • SANTA MONICA • CALIFORNIA

SUMMARY

The turbulent boundary-layer drag is studied for production-type or non-ideal aircraft surfaces. Stemming from the results of flight-test data for full-scale late-model aircraft; it has previously been concluded that there are no apparent Reynolds number effects on the zero-lift drag at flight speeds below the drag-rise Mach number. This independence of boundary layer drag on Reynolds number is made rational by reviewing the internal mechanism of the incompressible turbulent-boundary layer together with the basic empirical results; all as affected by surface roughness.

It is concluded from fundamental concepts that the effects of roughness elements protruding from the laminar sub-layer will increase the vorticity and thus increase the momentum losses in the turbulent boundary layer. This additional momentum loss, or drag, due to roughness has been shown from the empirical evidence to offset the decreasing skin friction drag as the Reynolds number increases.

Correspondingly, the above reasoning is extended to include the effects of compressibility in the turbulent boundary layer up to where the roughness elements themselves become locally affected and no longer are immersed in an incompressible field. As a consequence, for certain conditions, the compressible turbulent boundary layer drag for rough surfaces may also be considered independent of Reynolds number.

A recipe is presented for estimating the boundary layer drag contributions of practical aircraft insulated surfaces: Given a surface finish, an equivalent sand-grain roughness is determined from Table I. The incompressible boundary layer drag is then determined from Fig. 5 and corrected for Mach number by

Fig. 4. The resulting drag coefficients, C_{f_r} are independent of increasing Reynolds numbers, R_{e_ℓ}, for R_{e_ℓ} greater than critical, i.e., the R_{e_ℓ} at which C_{f_r} equals the drag due to pure skin friction, C_f.

$$C_f = \frac{0.472}{\left(\log_{10} R_{e_\ell}\right)^{2.5} \left(1 + \frac{\gamma-1}{2} M^2\right)^{0.467}} \qquad (13,14)$$

At R_{e_ℓ} less than critical the boundary drag is that of pure skin friction and given by the above relation. For a surface of given length, ℓ, measured streamwise having an external finish equivalent to a sand grain roughness, k_s, such that $k_s/\ell = 0.746 \times 10^{-5}$; the turbulent boundary-layer drag estimate shown in Fig. 3 may be prepared.

NOMENCLATURE

Symbol	Definition
x, y	coordinates parallel and normal to the surface respectively
u	local velocity in the x-direction
M	Mach number
τ	local boundary layer shear
ρ	local density
ℓ	turbulence mixing length
K	mixing length constant
k	mean surface-roughness height
k_s	sand grain diameter
c_f, C_f	local and average skin friction coefficient respectively
c_{f_r}, C_{f_r}	local and average rough-surface boundary layer drag coefficient respectively
A, B, C, n	constants
T	local boundary layer temperature
$\frac{dT_w}{dy} = 0$	insulated surface or boundary layer condition

Subscripts	Reference
w	wall or surface
∞	free stream

THE TURBULENT BOUNDARY-LAYER VELOCITY PROFILE-GENERAL DISCUSSION

The purpose of this section is to extrapolate the known effects of surface roughness in an incompressible turbulent boundary-layer to those for compressible flow regions. The mathematical difficulties encountered in the turbulent boundary-layer study field are responsible for a variety of approximate analyses which have been formed around two or three sets of original data. Although semi-empirical methods abound for describing the boundary-layer phenomenon, in the main they all rest upon a set of fundamental concepts intended to ease the mathematical treatment of an otherwise unsolvable problem. It is important to realize what the limitations are of these fundamental simplifications in order to assess the results predicted from their use.

Accordingly, the assumptions and accompanying analysis of the internal mechanism of the turbulent boundary-layer are reviewed. One important conclusion made is that due to the omission of the molecular viscous effects which are actually present at or near the wall in boundary-layer flow, the predicted magnitude of local velocities occurring in this vicinity are expected to be in excess of those physically realized.

Physically, the turbulent boundary-layer is divided into three regions of differing "viscous action" c.f. Fig. 1.

These regions are:

a. the laminar sub-layer (molecular diffusive forces only)

b. the buffer layer (molecular and eddy, or "fluid chunks", diffusive forces of comparable influence)

c. the turbulent domain (eddy diffusive forces predominate)

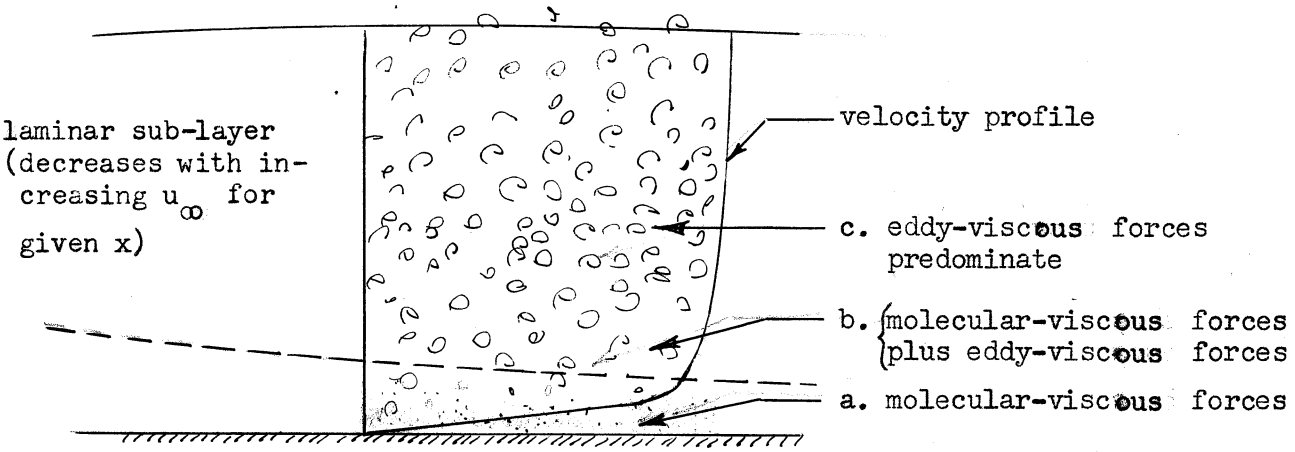

Fig. 1 THE TURBULENT BOUNDARY-LAYER REGIONS OF VISCOUS ACTION

In order that the equations of motion governing the momentum diffusion or energy change through the incompressible boundary layer be in a form suitable for solution, it becomes necessary to disregard the effects of molecular viscosity. Therefore, in Fig. 1, only the eddy forces or pure turbulence remain to affect the predicted conditions in the boundary layer.

The diffusion of the eddies create energy changes; this is due to the momentum changes occurring up through the boundary layer. The result is a local resistance force or apparent shear. The individual eddies involved in the diffusion, or random migrations, are considered to be solid bodies; therefore at each point in the boundary layer, the resistance force is then proportional to the square of the local velocity. Expressing the velocity by the gradient times a length, the local apparent shear is described by

$$\tau = \rho \ell^2 \frac{du}{dy} \left| \frac{du}{dy} \right| \qquad (1)$$

where ℓ is called the mixing length and represents the turbulence strength. Prandtl concludes a simple form for the mixing length

as $$\ell = K_1 y \tag{2}$$

where K_1 = constant. Eq. 2 is based on the physical observation that the vorticity strength decreases down through the boundary layer to zero at the wall.

Von Kármán's dimensional analysis of the mixing length concept results in

$$\ell = K_2 \left| \frac{\frac{du}{dy}}{\frac{d^2u}{dy^2}} \right| \tag{3}$$

where K_2 = constant. Eq. 3 results from considering the eddy migrations, at each point in the boundary layer, normal to the direction of the mean flow to be similar when the sizes of the fundamental dimensions of length and time are suitably changed.

It is repeated that both Eqs. 2 and 3 result from disregarding the energy dissipated by molecular viscosity.

Prandtl points out that according to Von Kármán's similarity theorem, the local average velocity near the wall must be of the form

$$u = A(y+B)^n + C \tag{4}$$

with A, B, C and n are constant. Thus from Eq. 3

$$\ell = K_3 (y+B) \tag{5}$$

where y is the center of similarity at each point in the boundary layer, and B is the constant which shifts the reference axis on which $\ell = 0$.

When Eq. 1 is integrated with Prandtl's mixing length relation, Eq. 2, considering constant shear throughout the region, there results for the local velocity

$$u = \sqrt{\frac{\tau}{\rho}}\ \frac{1}{K_1}\ \log y + \text{const.} \qquad (6)$$

Eq. 6 is known as the logarithmic law for the velocity distribution throughout the turbulent boundary-layer.

In Eq. 6, when $y = 0$, $u = -\infty$; this is contrary to the physical condition set by Eq. 2. Therefore, from the concept of similarity, $B > 0$ in Eq. 5, and the reference axis of similarity lies under the surface of the wall. At the wall $\ell > 0$ and therefore $u > 0$. Thus the velocity profile represented by Eq. 6 is seen to be that shown in Fig. 2.

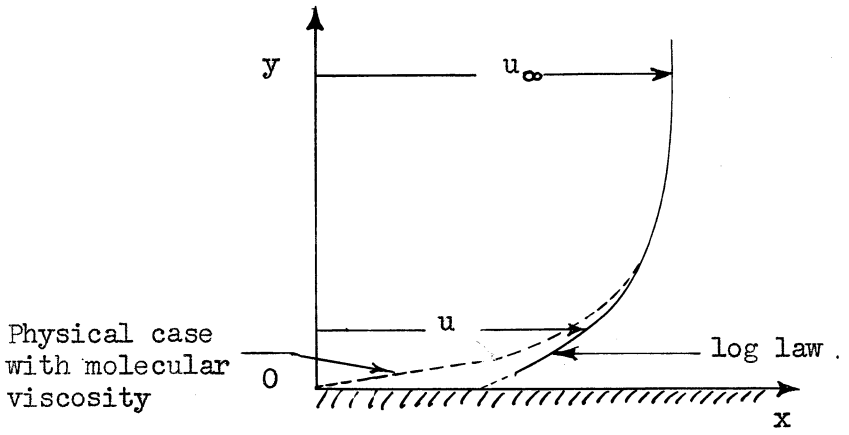

Fig. 2. TURBULENT BOUNDARY LAYER VELOCITY PROFILE

Actually it is known that the molecular viscous forces in the laminar sub-layer will halt the average fluid motion at the wall; therefore it is expected that all turbulent-flow velocity profiles at or near the wall will have actual values less than that predicted by present day analyses. This has been substantiated in all measurements that have been compared to analytical methods based on the mixing length concept.

THE TURBULENT BOUNDARY OVER A ROUGH SURFACE—INCOMPRESSIBLE FLOW

All turbulent boundary-layers include a relatively small laminar sub-layer adjacent to the solid wall. This region behaves as a blanket covering such surface defects as crevices, protruberances, and roughness. So long as surface irregularities are immersed within the low-velocity flow of the sub-layer, the over all effects are that of a smooth-wall creating pure skin friction drag.

When surface irregularities, particularly particles of roughness, extend outside the laminar sub-layer into the field of higher mean velocities, further momentum losses occur in the boundary layer. This additional roughness drag together with the pure skin friction or smooth-wall effect constitutes the total boundary-layer drag experienced by most practically-constructed and finished aircraft components.

To date, the only systematized experimental work on the effect of roughness exists for incompressible flow. Nikuradse, Ref. 1, worked with pipes that were artificially roughened with sand grains. His experiment showed that for a given roughness there exists a Reynolds number at which the measured boundary layer drag rises in value above a trend characterizing a pure skin friction effect. Furthermore, with increasing Reynolds number, the deviation from pure skin friction increases until a constant total drag value is reached. The total boundary-layer drag then becomes independent of Reynolds number and proportional to the square of the velocity. When the boundary-layer drag becomes independent of Reynolds number, fully developed roughness flow is said to exist.

The increasing roughness-drag phenomenon may be explained in two ways, both due to the thinning of the laminar sub-layer with increasing

Reynolds number. The first is that local flow separations are induced as portions of the surface emerge into the region of turbulence; this creates a pressure drag in the boundary layer. Apparently, for fully developed roughness flow, the additional drag increase negates the decreasing effect Reynolds number has on pure skin friction.

Another explanation of roughness drag is to consider that the particles emerge from the laminar sub-layer and shed additional vortices. The turbulence intensity is increased, but the mechanism of dispersion is the same as for a smooth-wall. Although the form of the mixing length equation would remain unaltered, the reference axis of similarity, B in Eq. 5, would change. Correspondingly, the velocity distribution for roughness flow would be similar in shape to the smooth-wall counterpart but of smaller local values.

Prandtl and Schlichting, Ref. 2, converted Nikuradse's results for sand roughened pipes to flat plate flow. The boundary layer drag coefficients for fully developed roughness flow over a flat plate may be represented by their interpolation formulas:

$$c_{f_r} = \left(2.87 + 1.58 \log_{10} \frac{\ell}{k_s}\right)^{-2.5} \tag{7}$$

$$C_{f_r} = \left(1.89 + 1.62 \log_{10} \frac{\ell}{k_s}\right)^{-2.5} \tag{8}$$

where c_{f_r} and C_{f_r} are the local and average coefficients respectively.

The velocity distribution in the turbulent boundary layer with fully developed roughness flow was derived by Prandtl, Ref. 3, from Nikuradse's data, and is

$$\frac{u}{\sqrt{\frac{\tau_w}{\rho}}} = 8.48 + 5.75 \log_{10} \frac{y}{k_s} \qquad (9)$$

where τ_w is the local shear at the wall and k_s is the average sand grain diameter. Eq. 9 is of the form of the logarithmic law, Eq. 6; this tends to substantiate the argument for the increased vorticity concept in explaining the mechanism of roughness flow.

C. THE TURBULENT BOUNDARY-LAYER OVER A ROUGH SURFACE—COMPRESSIBLE FLOW

Although the physical mechanism of roughness flow can be rationalized from two independent concepts, viz. induced pressure and the creation of additional eddies, it is more than likely that both properties contribute to the roughness drag. By virtue of the fully developed roughness drag data correlating with the logarithmic law for the velocity profile it is concluded that the increased vorticity effects predominate. Furthermore, the scale of the pressure contribution is not expected to increase unless the elements of roughness are subjected to critical local flow conditions wherein wave drag results. Therefore, in extending Eqs. 7 and 8 to boundary layers of a compressible medium and supersonic free stream flow, interest is first centered around local Mach numbers at the roughness elements.

As previously discussed, expressions for the boundary layer velocity profiles based on the turbulence mixing length concept, to the exclusion of molecular viscosity effects, will predict larger local velocities near the wall than can be physically realized. Therefore, any of the existing compressiblity extensions of Eq. 1 can be employed with the assurance that the predicted effects will be conservative (larger than expected).

In line with the above use is made of Van Driest's compressibility extension of Prandtl's apparent shear relation, Ref. 7. Van Driest's basic assumption is that Eq. 1 is locally valid and the density is allowed to vary throughout the boundary layer. Proceeding in the identical manner it can be shown that the momentum equation in the region of roughness is

$$\frac{1}{A}\mathrm{Sin}^{-1}\frac{2A^2\left(\frac{u}{u_\infty}\right)-B}{(B^2+4A^2)^{1/2}}+\frac{1}{A}\mathrm{Sin}^{-1}\frac{B}{(B^2+4A^2)^{1/2}}=\frac{1}{u_\infty}\sqrt{\frac{\tau_w}{\rho_w}}\left(8.48+5.75\log_{10}\frac{y}{k_s}\right) \tag{10}$$

where $$A^2=\frac{\frac{\gamma-1}{2}}{T_W/T_\infty} \quad \text{and} \quad B=\frac{1+\frac{\gamma-1}{2}M_\infty}{T_W/T_\infty}-1$$

making $y = k_s$, $u = (u\ \text{rough})_{\text{max.}}$ and Eq. 10 then becomes

$$\frac{\frac{1}{A}\mathrm{Sin}^{-1}\ 2A^2\frac{u_{\text{rough}}}{u_\infty}_{\text{max.}}-B}{(B^2+4A^2)^{1/2}}+\frac{1}{A}\mathrm{Sin}^{-1}\frac{B}{(B^2+4A^2)^{1/2}}=6\sqrt{c_{f_r}} \tag{11}$$

The energy equation is

$$\frac{T}{T_\infty}=\frac{T_w}{T_\infty}-\left(\frac{T_w}{T_\infty}-1\right)\frac{u}{u_\infty}+\frac{\gamma-1}{2}M_\infty^2\ \frac{u}{u_\infty}\left(1-\frac{u}{u_\infty}\right) \tag{12}$$

For present airplane considerations, interest in the boundary-layer compressibility effects does not extend beyond free stream Mach numbers of 2. Conservatively assuming that local Mach numbers below 0.4 at the tips of the roughness elements will not alter the incompressible roughness drag effects,

it is possible to determine the first-order maximum allowable degree of roughness before compressibility must be considered. Inasmuch as the boundary-layer temperature influences the local Mach numbers, two extreme cases of cooling and heating of the wall are considered; viz. temperature ratios

$$T_w/T_\infty = 1.0 \text{ and } 1.8 \text{ for } M_\infty = 2.0 \ .$$

From Eqs. 11 and 12, the local boundary layer drag coefficients are tabulated.

$M_{loc} = .4$ $M_\infty = 2.0$		
T_w/T_∞	u_{loc}/u_∞	c_{f_r}
1.0	.213	.0012
1.8	.260	.0019

It can be shown that by any of the compressibility factors available for ratioing the local boundary layer drag contribution of the above results to the incompressible values, and by substituting the equivalent $M = 0$ c_{f_r}'s into Eq. 7, the maximum allowable roughness not affected by compressibility are of the following orders of magnitude:

$M_{loc} = .4$ $M_\infty = 2.0$	
T_w/T_∞	k_s/ℓ
1.0	$0(10^{-7})$
1.8	$0(10^{-5})$

Therefore, due to the "smooth-wall" turbulence diffusion mechanism, the same compressibility corrections may be applied to rough-wall boundary-layers for free stream Mach numbers up to 2 with the equivalent sand roughness not exceeding ratios listed in the above table.

Fig. 3., shows the boundary layer drag for fully developed roughness flow as extended by the additional turbulence concept. All computations were carried out for an insulated boundary-layer and equivalent sand roughness ratio

$$k_{s/\ell} = 0.764 \times 10^{-5} \quad .$$

The dashed curves in Fig. 3 represent pure or smooth-wall turbulent skin friction according to Schlichtings' incompressible flow relation.

$$C_f = \frac{0.472}{(\log_{10} R_{e_\ell})^{2.5}} \tag{13}$$

modified for compressibility by Fig. 4. The curve of $C_f/C_{fM=0}$ vs M_∞ presented in Fig. 4 results from the analysis of Rubesin et al, Ref. 8. Included with the compressibility correction curve is a summary of some of the more valid experimental results. The agreement between the data and semi-empirical results justifies the selection of this particular curve. According to the results of the analysis in Ref. 8 , there is no Reynolds number effect for the skin friction parameters combined in the above manner.

Analogous to Eq. 13, the average drag coefficient for fully developed roughness and incompressible boundary-layer flow described by Eq. 8, Fig. 5, is corrected for Mach number by the relation.

$$\frac{c_{f_M}}{c_{f_{M=0}}} = \frac{C_{f_M}}{C_{f_{M=0}}} = \frac{1}{\left(1 + \frac{\gamma-1}{2} M_\infty^2\right)^{0.467}}, \quad M_\infty \leq 4 \tag{14}$$

of Fig. 4.

Therefore within the bounds of the present discussion, the boundary-layer drag coefficients may be described by the relations

$$c_{f_r} = \frac{\left(2.87 + 1.58 \log_{10} \frac{\ell}{k_s}\right)^{-2.5}}{\left(1 + \frac{\gamma-1}{2} M_\infty^2\right)^{0.467}} \tag{15}$$

$$C_{f_r} = \frac{\left(1.89 + 1.62 \log_{10} \frac{\ell}{k_s}\right)^{-2.5}}{\left(1 + \frac{\gamma-1}{2} M_\infty\right)^{0.467}} \tag{16}$$

As shown in Fig. 3, it is assumed that the turbulent boundary-layer flow abruptly changes from a smooth-wall condition to that with fully developed roughness. The Reynolds number at which this transition occurs being arbitrarily defined at that value at which the boundary-layer drag coefficient, C_{f_r}, is equal to the smooth-wall skin friction value, C_f.

THE DETERMINATION OF THE EQUIVALENT SAND GRAIN DIAMETER

As discussed in the previous section the application of the method for determining the boundary layer drag coefficients for non-ideal surfaces is based on the equivalent surface finish measured in sand grain diameters. Table I provides a summary of the types of surface finish correlated with the equivalent sand grain sizes. The correlation is a result of the combined researches of Colebrook and White, Hoerner, and Young; Refs. 9, 10, and 11, respectively.

TABLE I EQUIVALENT SURFACE FINISH

Type of Surface	k inches x 10^3	k_s inches x 10^3
Mirror Finish	0 - .049	0 - .079
Polished Metal or Wood	.05 - .09	.08 - .159
Natural Sheet Metal	.1 - .19	.16 - .319
Optimum Paint-Sprayed	.2 - .29	.32 - .479
Average Paint-Sprayed	.30 - .99	.48 - 1.59
Mass Production Paint-Sprayed	1.0 - 10	1.60 - 16.

One suggested method of approach is to determine the equivalent sand-grain diameter by proceeding backwards. From a known incompressible C_{D_r} of a given component having a surface finish representative of future designs, the k_s may be determined. With but a few samplings of each component, e.g., wing, fuselage, nacelles, reasonable estimates may then be made for projected configurations. Such contaminating items as leaks, isolated clusters of rivet heads, and the like would be implicit in the results.

FIG. 3 TURBULENT BOUNDARY LAYER FOR ROUGH SURFACES

INSULATED CASE

BOUNDARY LAYER DRAG COEFFICIENTS BASED ON NET WETTED AREA
EQUIVALENT SAND GRAIN ROUGHNESS RATIO $k_s/\ell = 0.746 \times 10^{-5}$

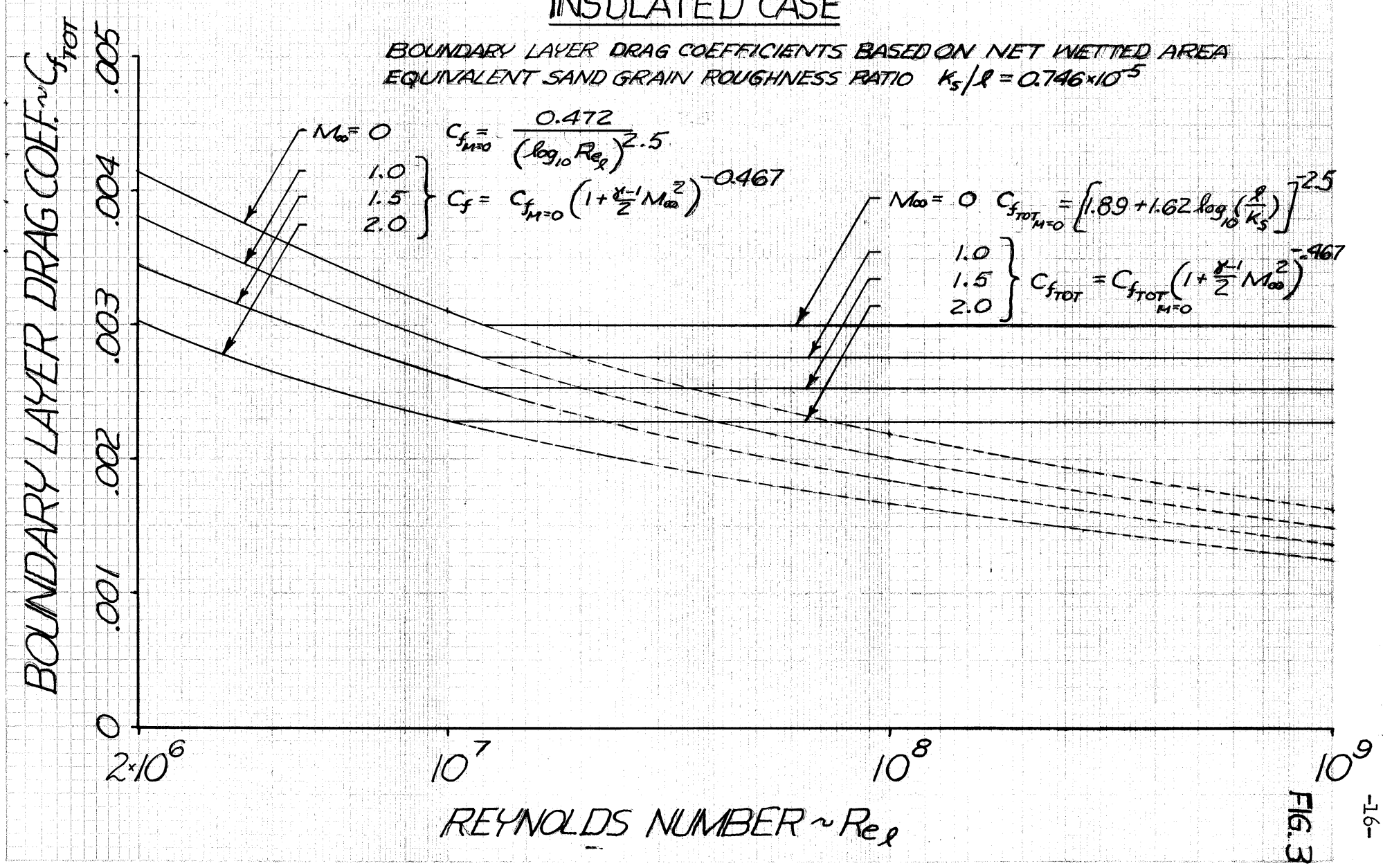

FIG. 3

FIG. 4 TURBULENT BOUNDARY LAYER COMPRESSIBILITY FACTOR INSULATED CASE

SYMBOL	$Re_\ell \times 10^{-6}$	AUTHOR	SOURCE
○	8	COLES	J.A.S. VOL. 19, NO. 10
□	7	RUBESIN, MAYDEW & VARGA	NACA TN 2305
◇	7	WILSON, YOUNG & THOMPSON	
▽	7	GINSBURGH	
⊖		WIESELSBERGER	
⊕		KEMPF	

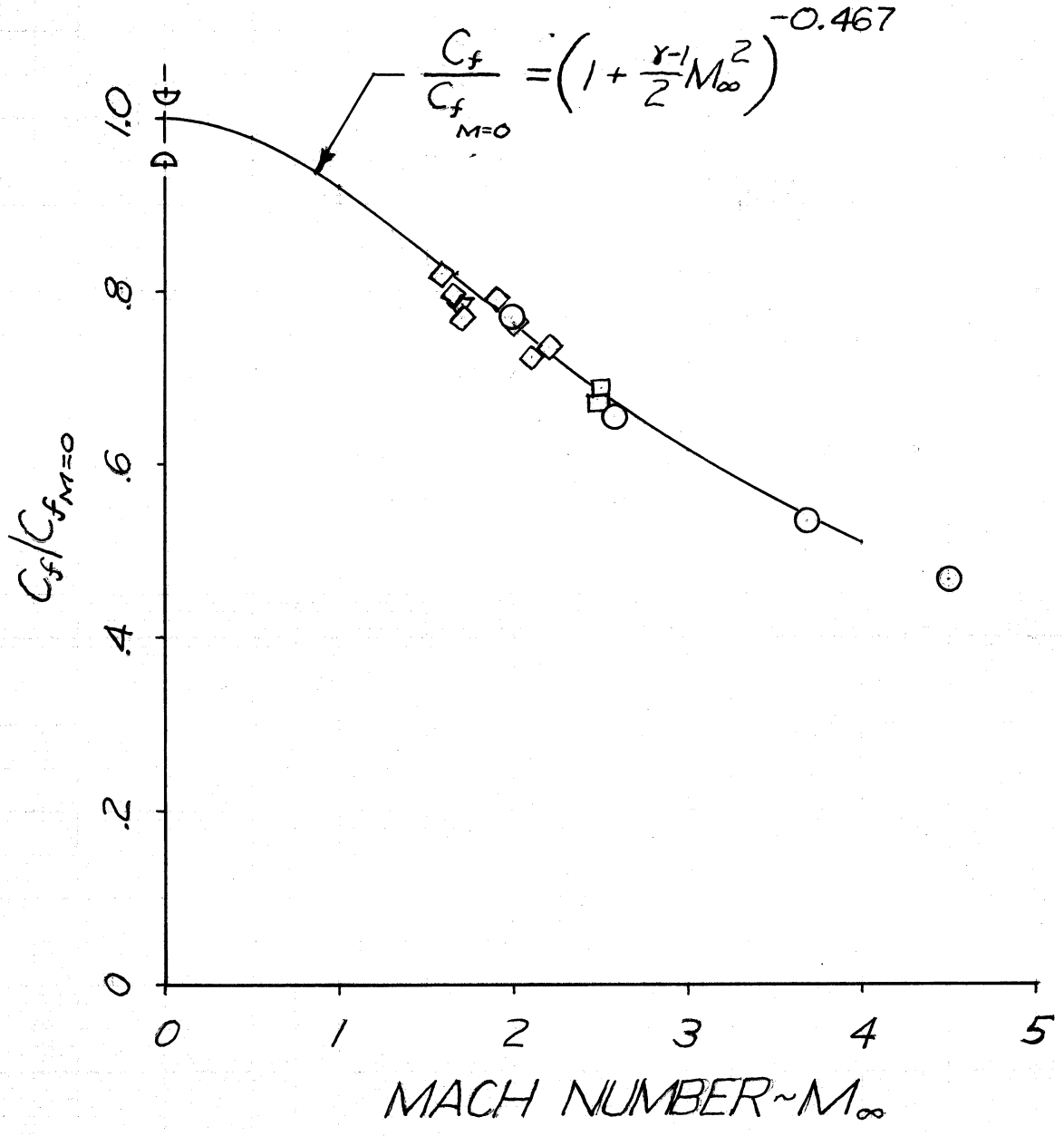

FIG. 5 INCOMPRESSIBLE BOUNDARY LAYER DRAG FOR ROUGH SURFACES

REFERENCE: PRANDTL, L., AND SCHLICHTING, H.: DAS WIDERSTANDSGESETZ RAUHER PLATTEN. WERFT, REEDEREI, HAFEN 1934. (NACA TM NO. 1218, APRIL 1949)

k_s ~ EQUIVALENT SAND GRAIN DIAMETER

l ~ CHARACTERISTIC LENGTH

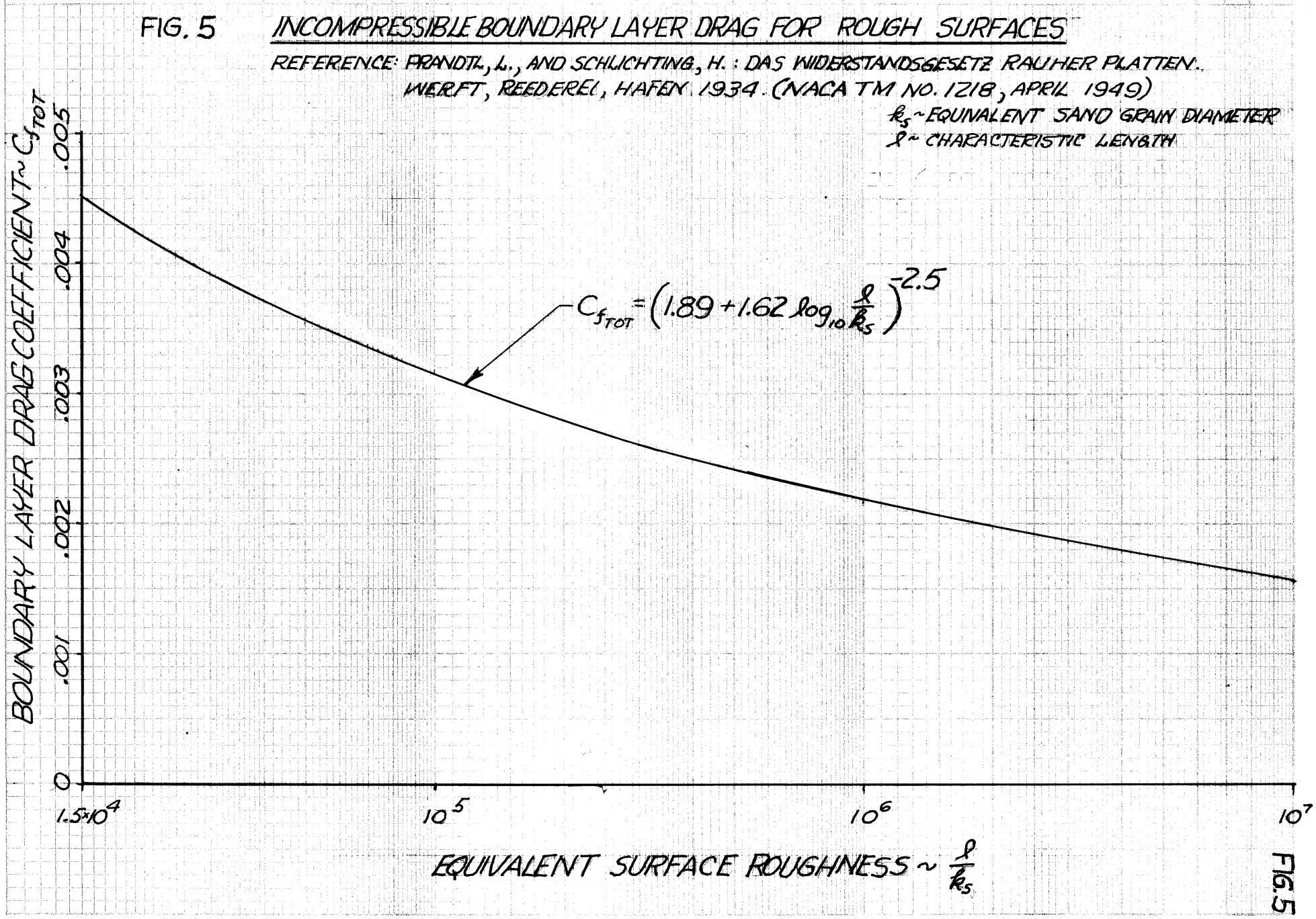

FIG. 5

REFERENCES

1. Nikuradse, J.: Strömungsgetsetze in rauher Rohren. Forschungsheft 361 des Vereins Deutscher Ingenieure, 1933. (NACA TM 1218, April, 1949)

2. Prandtl, L., and Schlichting, H.: Das Widerstandsgesetz rauher Platten. Werft, Reederei, Haften. 1934, p. 1.

3. Prandtl, L.: Zeitschrift des Vereines deutscher Ingenieure, 77 (1933), pp. 105-113.

4. Prandtl, L.: Zeitschr. f. angew. Math. u. Mech. 5(1925), 137, 138.

5. Nikuradse, J.: Strömung in glatten Rohren. Forschungsheft 356 des vereins Deutscher Ingenieure, 1932.

6. Durand, W.: Aerodynamic Theory, Vol. III, (1934) P. 139.

7. Van Driest, E. R.: Turbulent Boundary Layer in Compressible Fluids, Journal of the Aeronautical Sciences, Vol. 18, No. 3, March 1951..

8. Rubesin, M. W., Maydew, R. C., and Varga, S. A.: An Analytical and Experimental Investigation of the Skin Friction of the Turbulent Boundary Layer on a Flat Plate at Supersonic Speeds. NACA TN 2305, February 1951.

9. Colebrook, C. F., and White, C. M.: Experiments with Fluid Friction in Roughened Pipes, Proceedings of the Royal Society, Series A, Math. and Phys. Sciences, No. 906, 3 August 1937, Vol. 161, pp. 367-381.

10. Hoerner, S. F.: Aerodynamic Drag, The Otterbein Press, Dayton, Ohio, 1951, p. 45.

11. Young, A. D.: The Drag Effects of Roughness at High Sub-Critical Speeds, Journal of the Royal Aeronautical Society 54,(1950), pp. 534-540.